AIAA Aviation Forum and ASCEND co-located Conference Proceedings
21 - 25 July 2025, Las Vegas, Nevada
AIAA AVIATION FORUM AND ASCEND 2025

10.2514/6.2025-3078

Numerical simulations of guided jet waves

Christophe Bogey*
CNRS, Ecole Centrale de Lyon, INSA Lyon, Universite Claude Bernard Lyon I,
Laboratoire de Mécanique des Fluides et d'Acoustique, UMR 5509, 69130 Ecully, France

The acoustic waves that are mainly trapped into the potential core of jets, recently referred to as guided-jet waves (GJW), are investigated by performing numerical simulations of wave propagation. For that purpose, a single-frequency monopolar sound source is imposed on the axis of an isothermal round jet, modeled as a cylindrical shear layer. The waves radiated by the source are computed by solving the Euler equations. The shear-layer velocity profile is a hyperbolic-tangent profile, with a momentum thickness equal to 20 per cent of the jet half-width to avoid the rapid growth of Kelvin-Helmholtz instability waves. Three jet Mach numbers, namely $M = 0.75$, 0.95 and 1.10, and source Strouhal numbers ranging up to 2, 1.2, and 0.8, respectively, are considered. In the three cases, GJW belonging to the first two radial GJW axisymmetric modes are obtained. Depending on the frequency, they propagate in the upstream or in the downstream directions, and are entirely or partially contained in the flow. Their levels inside and outside the jet are represented in the frequency-wavenumber space. They are also quantified upstream and downstream of the source. They vary smoothly with the frequency for $M = 0.75$, but in a sharp and saw-tooth manner for $M = 0.95$ and 1.10. Outside the jet, their variations are consistent with the footprints left by the GJW in the sound spectra near the nozzle of jets.

I. Introduction

Many studies have been carried out in recent years on the waves that are essentially contained in the core of high-speed jet flows, often referred to as neutral acoustic waves, trapped or guided jet waves in the literature. As shown by Tam and Hu [1] using a linear-stability analysis nearly forty years ago, these waves have specific dispersion relations and eigenfunctions and can be classified into modes depending on their radial and azimuthal structures. The GJW propagating in the upstream direction, in particular, are only allowed in narrow frequency bands [2], and play a key role in the occurrence of resonance phenomena [3, 4]. They can close the feedback loops in jets impinging on a plate [5–8], in jets interacting with an edge [9] or a flat plate [10, 11], in screeching shock-containing jets [12–14] and in supersonic twin jets [15]. For non-screeching free jets, they also lead to the generation of peaks in the pressure spectra near the nozzle exit [16–19], as illustrated in figures 1(a-c) for jets at Mach numbers 0.60, 0.90 and 1.10 for the axisymmetric mode $n_\theta = 0$, and in the acoustic far field in the upstream direction [20–22]. The peaks have a tonal, saw-tooth shape in figures 1(b,c) for the two highest Mach numbers, which has been attributed to the establishment of resonance in the jet potential core [23–25] between upstream- and downstream-travelling GJW, that can both exist for Mach numbers typically above 0.80. Finally, for jets with laminar nozzle-exit conditions, the GJW excite the shear-layer instability waves near the nozzle [26].

The dispersion relations and eigenfunctions of the GJW are usually determined using a vortex-sheet model assuming an infinitely thin mixing layer [1]. The dispersion relations obtained in this way for jet Mach numbers $M = u_j/c_0 = 0.75$, 0.95 and 1.10 are, for example, represented in figures 2(a-c) as functions of axial wavenumber k_z and Strouhal number $\mathrm{St}_D = fD/u_j$, where f is the frequency, D and u_j are the jet nozzle-exit diameter and velocity and c_0 is the speed of sound in the ambient medium. The limit points L of the dispersion curves on the sonic line $k_z = -\omega/c_0$, where ω is the pulsation, the inflection points I, and the stationary points S_{min} and S_{max} are also indicated. Depending on the position on the curves, the group velocities of the waves are negative or positive, leading to upstream and downstream directions of propagation, respectively. The radial profiles of the GJW also vary significantly [1, 23]. The waves have a non-negligible support outside the jet near $k_z = -\omega/c_0$, but are fully confined to the jet flow near $k_z = \omega/(u_j - c_0)$. Thus, they can be referred to as free-stream GJW in the first case and as duct-like GJW in the second. The predictions of the vortex-sheet model, in terms of GJW dispersion curves and eigenfunction distributions, are in most cases in good agreement with the data from the experiments and simulations. This is exemplified in figures 1(b,c), where the

*CNRS Research Scientist, christophe.bogey@ec-lyon.fr, AIAA Associate Fellow.

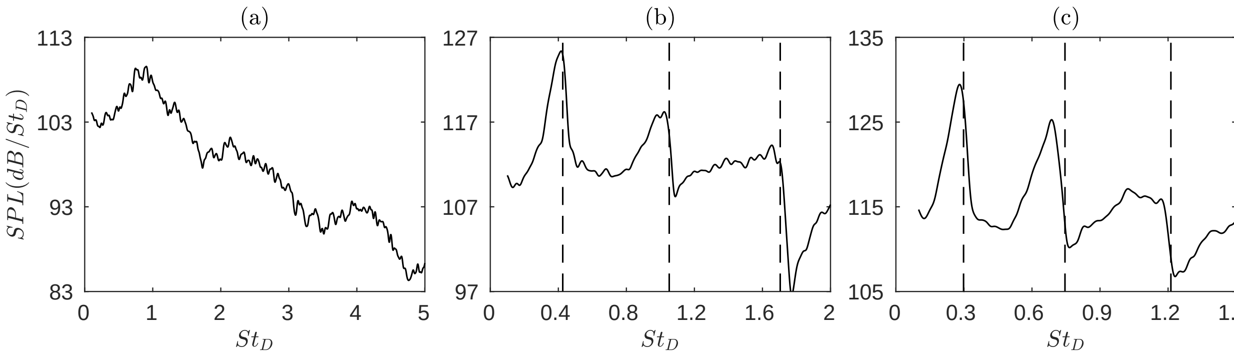

Fig. 1 Sound pressure levels [18] obtained near the nozzle of jets at (a) M = 0.60, (b) M = 0.90 and (c) M = 1.10 for $n_\theta = 0$ as a function of Strouhal number St_D; − − − St_D at points S_{max} on the GJW dispersion curves for a vortex sheet.

abrupt decreases after the peaks in the near-nozzle spectra occur very near the frequencies of the stationary (or saddle) points S_{max} of the dispersion curves of the first radial GWJ modes for $n_\theta = 0$. The use of finite-thickness mixing-layer models may, however, be necessary for very thick shear layers [3, 6, 27, 28]. Moreover, the models mentioned above provide no information on the GJW amplitudes other than the normalized eigenfunction profiles.

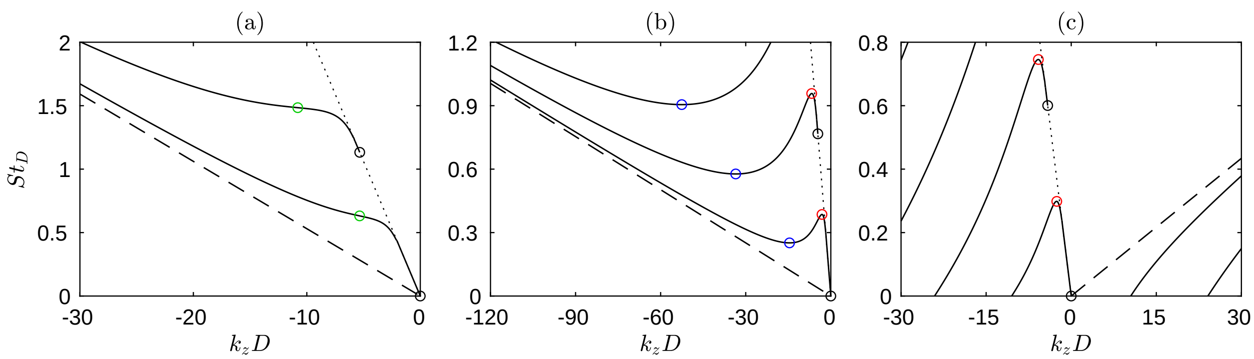

Fig. 2 GJW dispersion curves obtained for $n_\theta = 0$ at (a) M = 0.75, (b) M = 0.95 and (c) M = 1.10 using the vortex-sheet model as a function of k_zD and St_D; points ∘ L, ∘ S_{max}, ∘ S_{min} and ∘ I; − − − $k_z = \omega/(u_j - c_0)$, ⋯⋯ $k_z = -\omega/c_0$.

On the basis of the above, numerical simulations are performed in the present work to directly compute GJW in jets with finite-thickness mixing layer, with the aim of getting access to all their properties including their true, non-normalized amplitudes. The GJW are investigated by considering them only as the result of a problem of acoustic propagation in presence of a sheared flow. That was previously the case in the simulations of the propagation of random noise fluctuations and of a pressure pulse in a jet flow by Bogey and Gojon [6] and Bogey [29], and in the theoretical analyses of the scattering of acoustic waves through single- and double-vortex sheets by Martini et al. [30] and Nogueira et al. [31]. The study of Nogueira et al. [31], in particular, demonstrated that the GJW can only result from acoustic waves generated in the core of the flow. These waves were shown to experience internal reflection and transmission from the two shear layers behaving like a soft-duct, for a given range of frequencies and wavenumbers, the phase of the reflection coefficient determining the wavenumbers of the GJW. Transmission of the waves to the outside was also found to be maximum near the sonic line and to rapidly decrease as the waves become subsonic, explaining the formation of partially or fully confined GJW modes.

In this work, a monopolar sound source radiating at a single Strouhal number St_D is placed on the axis of a jet modeled as a cylindrical shear layer in order to generate axisymmetric GJW. The propagation of the waves radiated by the source is computed by solving the Euler equations using low-dissipation low-dispersion finite differences. To deal with the GJW of different kinds that can exist, three jet Mach numbers M, namely two high subsonic ones and a supersonic one, and a great number of Strouhal numbers are considered. The Strouhal number ranges are chosen to obtain GJW belonging to the first two radial GJW axisymmetric modes. Moreover, the source amplitude is small and the shear layer is very thick in order to prevent or inhibit the development of Kelvin-Helmholtz instability waves downstream of the source. In each case (M, St_D), the objective will be to ascertain whether GJW travel in the jet flow, and if so, to determine their directions of propagation and their amplitudes inside and outside the flow. Then, for a given Mach number, the variations of the GJW amplitude with the Strouhal number will be quantified and compared with those observed in the near-nozzle spectra of jets. The presence of tonal-like characteristics at specific GJW frequencies will especially be sought.

The paper is organized as follows. In section II, the jet flow conditions and the properties of the acoustic source placed in the flow are defined. The numerical methods and parameters are also documented. In section III, the results obtained for the three Mach numbers are presented. Finally, concluding remarks are given in section IV.

II. Parameters

A. Jet flow and acoustic source

In this study, three isothermal round free jets, two at subsonic Mach numbers $M = 0.75$ and 0.95 and one at a supersonic Mach number of $M = 1.10$, are considered. To generate acoustic waves, and possibly GJW in the flow, a single-frequency monopolar acoustic source is imposed on the jet axis at the axial position $z = 0$. According to the dispersion curves obtained for a vortex sheet in figure 2, the group velocities $v_g = \partial\omega/\partial k_z$ of the GJW are all negative for $M = 0.75$, but negative or positive for $M = 0.95$ and $M = 1.10$. Therefore, the GJW can be expected to travel only in the upstream direction in the first case, but upstream or downstream in the two other ones.

For simplicity, the jets consist of a cylindrical shear layer, surrounded by a medium at rest at temperature $T_0 = 293$ K and pressure $p_0 = 10^5$ Pa. Following Michalke [32], the radial profile of the axial velocity u_z is defined by the hyperbolic-tangent profile

$$u_z(r) = \frac{u_j}{2}\left\{1 + \tanh\left[\frac{r_0}{4\delta_\theta}\left(\frac{r_0}{r} - \frac{r}{r_0}\right)\right]\right\}$$

where u_j, $r_0 = D/2$ and δ_θ are the velocity on the axis at $r = 0$, the jet half-width and the shear-layer momentum thickness. The jet radial and azimuthal velocities are equal to zero, the jet pressure is equal to p_0 and temperature is determined by a Crocco-Busemann relation. The momentum thickness is set to $\delta_\theta = 0.20r_0$, yielding the thick velocity profile represented in figure 3(a). The value of δ_θ/r_0 is very large, which will most probably lead to differences relative to the predictions of the vortex-sheet model. It was chosen to avoid the presence of strong Kelvin-Helmholtz (KH) instability waves in the jet flows. Indeed, such waves might pollute the pressure fields, in particular if they result in the formation and pairing of vortical structures in the shear layers, which could make the extraction of the GJW characteristics difficult.

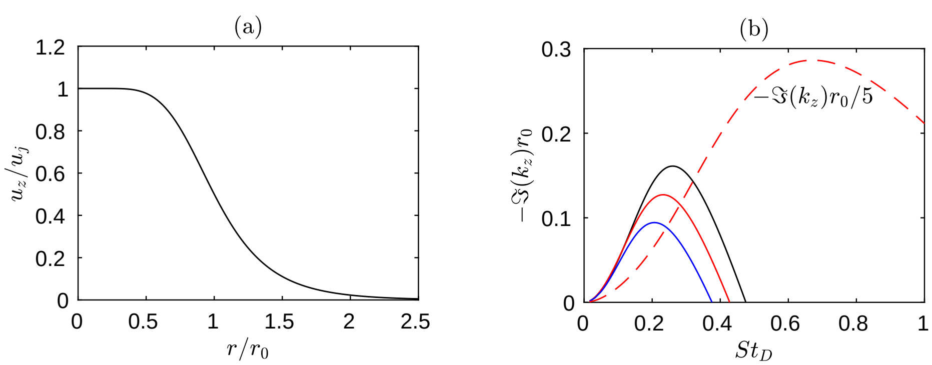

Fig. 3 Representation of (a) the profile of axial velocity u_z/u_j for $\delta_\theta = 0.20r_0$ and (b) the KH instability growth rates $-\Im(k_z)r_0$ obtained for that profile for $n_\theta = 0$ using linear stability analysis for —— $M = 0.75$, —— $M = 0.95$ and —— $M = 1.10$; – – – $-\Im(k_z)r_0/5$ for $M = 0.95$ and $\delta_\theta = 0.05r_0$.

In support of the latter claim, the amplification rates $-\Im(k_z)r_0$ of the KH instability waves obtained for the azimuthal mode $n_\theta = 0$ for the velocity profile using linear stability analysis (LSA) are represented in figure 3(b) as a function of Strouhal number St_D. Above $\mathrm{St}_D = 0.47$ for $M = 0.75$, $\mathrm{St}_D = 0.43$ for $M = 0.95$ and $\mathrm{St}_D = 0.38$ for $M = 1.10$, the amplification rates are negative, indicating that no instability waves should grow. This is particularly true in the frequency range of the second axisymmetric GJW modes according to figures 2(a-c). For lower Strouhal numbers, the amplification rates are weak. For instance, they are approximately ten times weaker than those predicted for $\delta_\theta = 0.05r_0$, shown in the figure. As a result, it is most likely that KH instability waves develop, but so slowly that their amplitudes remain small.

To check that, the pressure fields obtained for a source radiating at the most unstable Strouhal number for the three Mach numbers are provided in figures 4(a-c). KH instability waves are observed to grow downstream of the source, with amplitudes reaching only 1-2 Pa at $z = 30r_0$, a position from which a sponge zone is implemented. Their entry in this zone does not seem to generate spurious acoustic waves travelling in the upstream direction. It can also be noted that for the low Strouhal numbers $St_D \simeq 0.2$ considered, no GJW appear for $M = 0.75$ and 0.95, but that GJW are clearly found downstream of the source for $M = 1.10$.

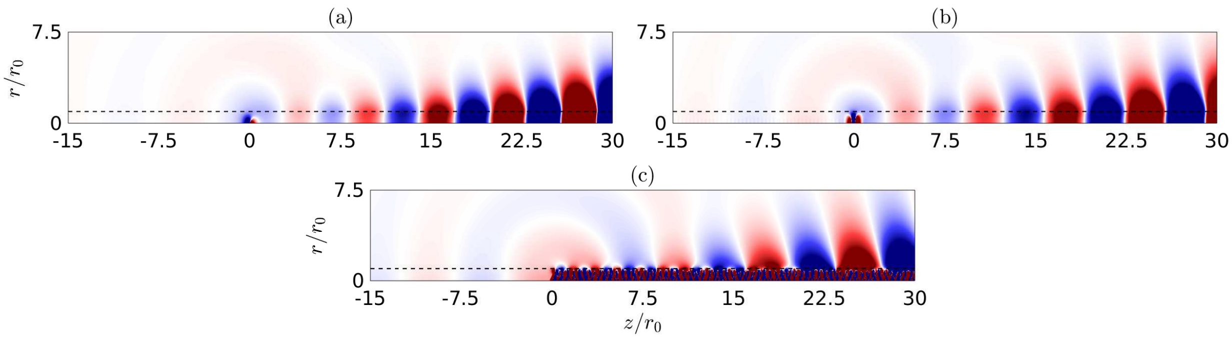

Fig. 4 Pressure fluctuations obtained for (a) $M = 0.75$ at $St_D = 0.26$, (b) $M = 0.95$ at $St_D = 0.23$ and (c) $M = 1.10$ at $St_D = 0.205$. The color scale levels range between ±0.1 Pa, from blue to red; − − − $r = r_0$.

The acoustic source on the jet axis at $z = 0$ and $r = 0$ has a Gaussian shape and a half-width of $3\Delta z(z = 0) = 3\Delta r(r = 0) = 0.06r_0$, where Δz and Δr are the grid spacings in the axial and radial directions. Its half-width is much smaller than the wavelength of the waves travelling at the ambient speed of sound, the smallest one being equal to $\lambda = 1.33r_0$ for $M = 0.75$ and $St_D = 2$, ensuring acoustical compactness. Its amplitude is very low to avoid non-linear effects during the wave propagation and the generation of KH instability waves of high intensity when the latter grow. For instance, the root-mean-square (r.m.s.) value of pressure fluctuations obtained at $10r_0$ from the source is equal to 1.8×10^{-3} Pa, corresponding to a sound pressure level of 39 dB.

The time evolution of the source amplitude is driven by a sinusoidal function of frequency $f_s = 1/T_s$, which is initially weighted by a half-Gaussian function increasing between $t = 0$ and $t = 30T_s$. The frequencies considered in the simulations are distributed over the Strouhal number ranges $0.10 \leq St_D \leq 2$ for $M = 0.75$, $0.10 \leq St_D \leq 1.20$ for $M = 0.95$ and $0.10 \leq St_D \leq 0.80$ for $M = 1.10$, in which GJW belonging to the first two radial axisymmetric GJW modes are expected. To accurately describe the variations of the GJW properties, the number of source Strouhal numbers n_{source} is significant, and is equal to 192 for $M = 0.75$, 271 for $M = 0.95$ and 182 for $M = 1.10$. In the last two cases, they are specially clustered around the Strouhal numbers of the stationary points S_{min} and S_{max} of the GJW dispersion curves, around which tonal components due to GJW are observed in jet near-nozzle spectra.

B. Numerical methods and parameters

The computations are carried out by solving the full Euler equations in cylindrical coordinates (r, θ, z) using the same numerical framework based on explicit high-order schemes as in previous simulations of spatially-developing [18, 26] and temporally-developing [33, 34] round jets. The axis singularity is taken into account by the method of Mohseni and Colonius [35]. Fourth-order eleven-point centered finite differences are used for spatial discretization, and a second-order six-stage Runge-Kutta algorithm is implemented for time integration [36]. A twelfth-order centered filter is applied explicitly to the flow variables every time step to remove grid-to-grid oscillations. Non-centered finite differences and filters are used at the grid lateral boundaries [37], where the radiation conditions of Tam and Dong [38] are applied. Periodic conditions are implemented at the inflow and outflow boundaries. Near these boundaries, sponge zones based on grid stretching and Laplacian filtering are built to move the periodic conditions very far from the region where wave propagation will be investigated.

C. Numerical parameters

The same mesh grid is used in all the simulations for $M = 0.75$ and in most ones for $M = 0.95$ and $M = 1.10$. In the axial direction, it is symmetrical relative to the source position $z = 0$, and extends, excluding the 260-point inflow and outflow sponge zones, between $z = -30r_0$ and $30r_0$. In this region, the mesh spacing Δz is uniform and equal to $0.02r_0$, providing a wavenumber $k_z r_0 = 63$ for 5 points per wavelength (PPW). In the sponge zones, the mesh spacing is stretched at a rate of 3%, leading to grid boundaries located at $z = \pm 880r_0$. In the radial direction, the mesh grid extends out to $r = 25r_0$. The mesh spacing Δr is also equal to $0.02r_0$ between $r = 0$ and $1.2r_0$. It then increases at a stretching rate of 2.6% up $r = 6.5r_0$, where $\Delta r = 0.16r_0$, yielding $St_D = 3.3$, 2.6 and 2.3 for an acoustic wave with 5 PPW propagating in the ambient medium for $M = 0.75$, $M = 0.95$ and $M = 1.10$, respectively. The radial mesh spacing finally grows again at the rate of 2.6% between $r = 16r_0$ and $21.6r_0$, to obtain $\Delta r = 0.32r_0$ near the boundary. Thus, the grid contains $N_z = 3,519$ points in the axial direction and $N_r = 235$ points in the radial direction. Given that the flow and the sound waves are axisymmetric, only $N_\theta = 2$ points are used in the azimuthal direction, and the derivatives in that direction are not calculated but set to zero.

For a source radiating in the Strouhal number ranges $0.38 \leq St_D \leq 0.4075$ and $0.90 \leq St_D \leq 0.975$ for $M = 0.95$ and $0.66 \leq St_D \leq 0.735$ for $M = 1.10$, upstream- and downstream-propagating GJW are found to both exist, which might cause spurious reflections in the sponge zones. To avoid this, the simulations are carried out using grids longer in the axial direction, containing more points in the central region where $\Delta z = 0.02r_0$. This region extends between $\pm 70r_0$ for $M = 0.95$ and $\pm 90r_0$ for $M = 1.10$, requiring 4,000 and 6,000 additional points, respectively. In these simulations, the absence of GJW reflected back in the computational domain by the sponge zones from outcoming KH instability waves or GJW has been checked using wavenumber-frequency analyses.

The simulations are performed with an OpenMP-based in-house solver on single nodes containing 16 to 64 cores, using a time step $\Delta t = CFL \times \Delta r(r = 0)/c_0$ with a Courant-Friedrichs-Lewy number $CFL = 0.70$ for $M = 0.75$, 0.65 for $M = 0.95$ and 0.60 for $M = 1.10$ to ensure numerical stability. After $t = 30T_s$, they run during a time of $120r_0/|u_j - c_0|$ to allow the GJW with a very group velocity, especially those near the stationary points S_{min} and S_{max} in the dispersion curves of figures 2(b,c), to travel over large distances. Then, pressure is recorded during $100T_s$ in the azimuthal plane $\theta = 0$ at every second point in the axial and radial directions between $z = \pm 30r_0$ and $r = 0$ and $30r_0$, at a sampling frequency corresponding to a Strouhal number $\mathrm{St}_D = 6.4$, and along the lines $r = 0$, $r = r_0$ and $r = 2r_0$ at every second point between $z = \pm 30r_0$ at a double frequency.

III. Results

In this section, results obtained for the three jet Mach numbers are presented. First, fields of pressure fluctuations are shown in the (z, r) section for several source frequencies to visualize the GJW that may form. Second, the levels of the pressure fluctuations recorded on the lines $r = 0$ and $r = 2r_0$ are examined in order to highlight the properties of the GJW inside and outside the jet flow. They are first represented in the wavenumber-frequency space, then as a function of the Strouhal number only for two specific positions upstream and downstream of the source.

A. Pressure fields at specific source frequencies

Snapshots of pressure fluctuations $p - p_0$ obtained for $M = 0.75$, 0.95 and 1.10 in (z, r) sections restricted to the near-source region are provided in figures 5, 6 and 7, respectively. For each Mach number, 12 Strouhal numbers are considered. They vary between $St_D = 0.98$ and 1.86 for $M = 0.75$, $St_D = 0.57$ and 1.03 for $M = 0.95$, and $St_D = 0.40$ and 0.73 for $M = 1.10$. In these frequency ranges, GJW belonging to the first and second radial axisymmetric GJW modes are expected according to the dispersion curves in figure 2. No KH instability waves should also grow according to the amplification rates predicted using LSA of figure 3(b). Indeed, no such waves appear downstream of the source in figures 5-7. In all cases, the source on the jet axis radiates waves that are transmitted outside of the flow. These waves are of oval form due to convection and refraction effects and have amplitudes of the order 10^{-2} Pa close to the source, decreasing rapidly with the distance as they propagate as three-dimensional acoustic waves.

More importantly, in certain cases, intense GJW are clearly observed upstream or downstream of the source. When they exist, their amplitudes on the jet axis greatly exceed 10^{-1} Pa, and sometimes even reach nearly 10 Pa, as in figure 6(j) for $M = 0.95$ and in figure 7(k) for $M = 1.10$, which is three orders of magnitude higher than the amplitudes of the sound waves outside the flow. The amplitudes of the GJW do not change much with the distance to the source, which supports that they are acoustic neutral waves [1] trapped into the jet due to total internal reflection [31]. The presence, directions of propagation, axial wavelengths and radial supports of the waves strongly depend on the Mach and Strouhal numbers. In particular, their amplitudes can be negligible or significant for $r > r_0$, indicating that they

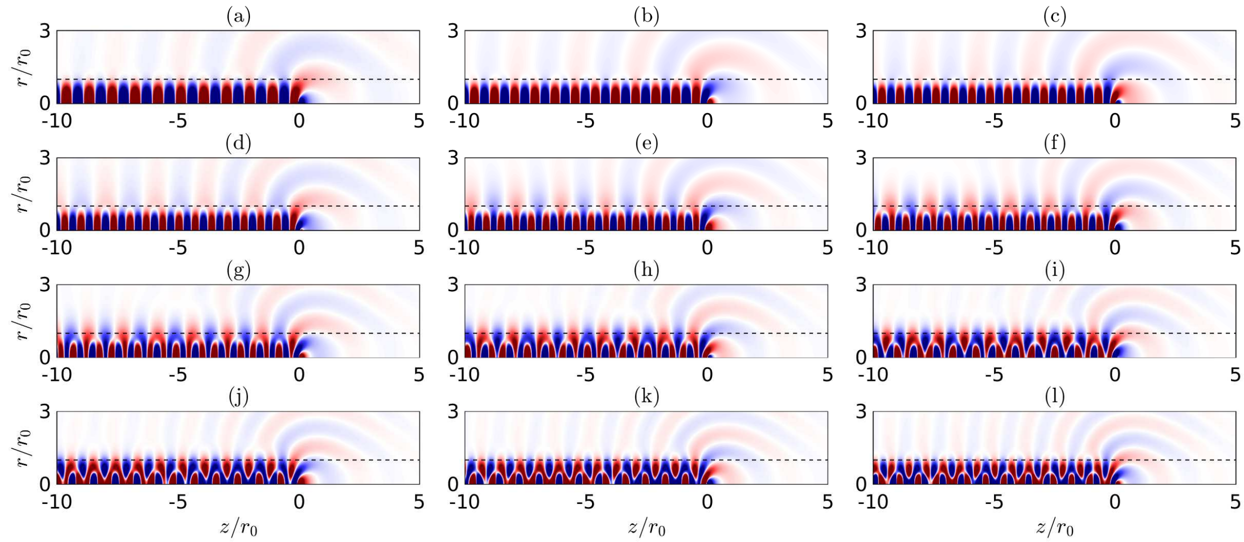

Fig. 5 Pressure fluctuations obtained for $M = 0.75$ at Strouhal numbers (a) 0.98, (b) 1.06, (c) 1.14, (d) 1.22, (e) 1.30, (f) 1.38, (g) 1.46, (h) 1.54, (i) 1.62, (j) 1.70, (k) 1.78 and (l) 1.86. The color scale levels range between ±0.1 Pa, from blue to red; − − − $r = r_0$.

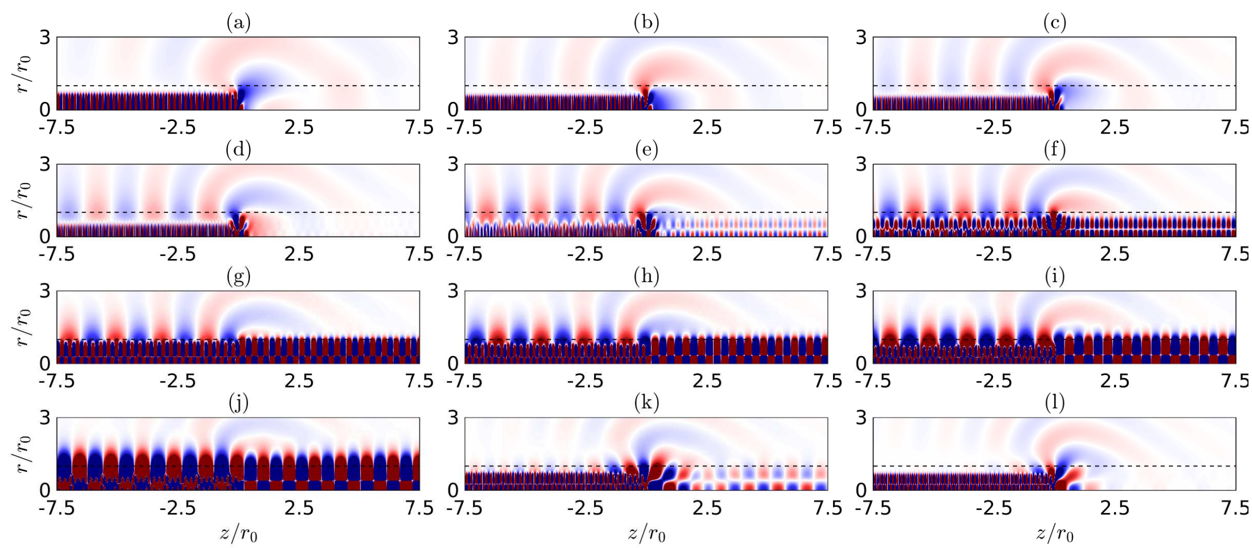

Fig. 6 Pressure fluctuations obtained for $M = 0.95$ at Strouhal numbers (a) 0.57, (b) 0.69, (c) 0.77, (d) 0.83, (e) 0.87, (f) 0.89, (g) 0.91, (h) 0.93, (i) 0.95, (j) 0.97, (k) 0.99 and (l) 1.03. The color scale levels range between ±0.1 Pa, from blue to red; − − − $r = r_0$.

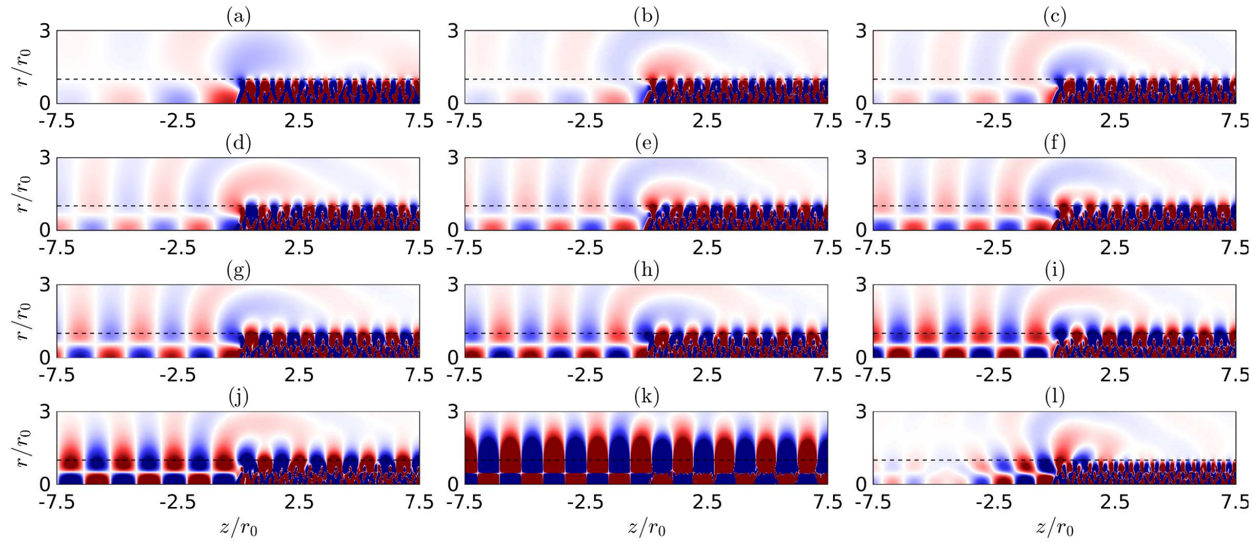

Fig. 7 Pressure fluctuations obtained for $M = 1.10$ at Strouhal numbers (a) 0.40, (b) 0.49, (c) 0.55, (d) 0.595, (e) 0.625, (f) 0.64, (g) 0.655, (h) 0.67, (i) 0.685, (j) 0.70, (k) 0.715 and (l) 0.73. The color scale levels range between ±0.1 Pa, from blue to red; − − − $r = r_0$.

are fully or partially trapped in the jet flow or, in other words, that they are duct-like or free-stream GJW [1, 9, 23]. None or one node can also be found in the pressure distributions of the waves in the radial direction, suggesting that they belong to the first or second radial axisymmetric GJW modes.

The variations of the GJW characteristics in the pressure snapshots with the source frequency are described below for the three Mach numbers.

For $M = 0.75$, over the Strouhal number range $0.98 \leq St_D \leq 1.86$ considered in figures 5(a-l), GJW are found upstream of the source in all cases, but never downstream. In figure 5(a) for $St_D = 0.98$, they are confined to $r \leq r_0$ inside the jet flow and their radial structure exhibits no node. As the source Strouhal number increases, the radial supports of the waves spread out of the jet at $r > r_0$, reaching approximately $r = 3r_0$ in figure 5(e) for $St_D = 1.30$, and then narrow until the waves are fully contained into the jet again. In the same time, the amplitudes of the GJW outside the jet flow grow and then decay. Thus, at $r = 1.5r_0$ for instance, they are significant in figure 5(g) for $St_D = 1.46$, but are negligible in figure 5(l) for $St_D = 1.86$. A node also appears in the radial support of the waves typically above $St_D = 1.22$.

For $M = 0.95$, over $0.57 \leq St_D \leq 1.03$ in figures 6(a-l), GJW are visible upstream of the source in all cases, but downstream only in figures 6(f-j) for $0.89 \leq St_D \leq 0.97$. Upstream of the source, the variations of the GJW properties with the frequency bear strong similarities with those reported above for $M = 0.75$. However, the peak values of the GJW amplitudes outside of the jet flow, obtained in figure 6(j) for $St_D = 0.97$, are much stronger in this case. Downstream of the source, when the GJW exist, a node is observed in their radial supports. As the Strouhal number increases, their supports, initially limited to $r < r_0$, extend farther from the jet axis well beyond $r = r_0$. The amplitudes of the waves outside of the jet grow and reach their highest values in figure 6(j) for $St_D = 0.97$. Therefore, the strongest upstream- and downstream-propagating GJW are found at the same Strouhal number.

Finally, for the supersonic Mach number $M = 1.10$, over $0.40 \leq St_D \leq 0.73$ in figures 7(a-l), GJW can be seen upstream and downstream of the source in all but one case, the exception being the absence of upstream-propagating GJW in figure 7(l) for $St_D = 0.73$. Upstream of the source, when they exist, the amplitudes of the GJW are nil around $r = 0.6r_0$ and similar on both sides of $r = r_0$ inside and outside of the jet flow. They are weak in figure 7(a) for $St_D = 0.40$ and spectacularly grow with the Strouhal number, leading to very high values in figure 7(k) for $St_D = 0.715$. Downstream of the source, the pressure fluctuations inside the jet are strong in all cases. Outside the jet, the amplitudes of the GJW are negligible in figure 7(a) for $St_D = 0.40$, and increase with the frequency, to reach intense values also in figure 7(k) for $St_D = 0.715$ before collapsing. In this figure, the upstream- and downstream-propagating GJW look very similar. They resemble those emerging in figure 6(j) for $M = 0.95$ at $St_D = 0.97$.

B. Acoustic levels on the lines $r = 0$ and $r = 2r_0$ in the wavenumber-frequency space

To explain the properties of the GJW in the pressure fields, the pressure fluctuations recorded between $z = \pm 30r_0$ on the lines $r = 0$ and $r = 2r_0$ are analyzed in the $k_z - St_D$ space. In practice, for each simulation performed at a source Strouhal number St_{Di} ($i \in [1, n_{source}]$), a wavenumber-frequency transform is applied to the signals, providing spectra from which the sound pressure levels $SPL_i(k_z)$ at St_{Di} are extracted. For a given Mach number and a given radial position, the levels $SPL_i(k_z)$ obtained from all simulations are then gathered in a matrix $[SPL_1; SPL_2; ...; SPL_{n_{source}}]$, yielding a spectrum that is represented a function of k_z and $St_D = [St_{Di=1,n_{source}}]$.

The spectra thus determined from the pressure fluctuations at $r = 0$ and $r = 2r_0$ are provided in figures 8(a,b) for $M = 0.75$, figures 9(a,b) for $M = 0.95$ and figures 10(a,b) for $M = 1.10$. For the three Mach numbers, high levels emerge in the spectra obtained at $r = 2r_0$ for positive wavenumbers in a spot elongated along the convection line $k_z = \omega/(0.7u_j)$. They are restricted to the Strouhal number ranges where KH instability waves develop according to the amplification rates in figure 3(b), whose upper bounds are shown. They are also strongest near the Strouhal numbers of maximum amplification rate, namely $St_D = 0.26$ for $M = 0.75$, $St_D = 0.23$ for $M = 0.95$ and $St_D = 0.205$ for $M = 1.10$. Therefore, they are due to the instability waves growing in the jet downstream of the source.

High levels are also found in the spectra for negative wavenumbers at $M = 0.75$ and 0.95, and for both negative and positive wavenumbers at $M = 1.10$, organized along a few distinct curves. These curves resemble the dispersion curves of the GJW obtained for mode $n_\theta = 0$ using a vortex-sheet model, also displayed. This strongly suggests that they result from the GJW that may form upstream and downstream of the source. The agreement between the numerical and theoretical curves is fair for the first radial mode $n_r = 1$ but quite poor for the modes $n_r > 1$, which can be attributed to the fact that the jet shear layer is very thick in the simulations but is infinitely thin in the model [3, 6, 27, 28].

Along the curves, the levels vary appreciably, depending on the radial position. At $r = 2r_0$, in figures 8(b), 9(b) and 10(b), they are significant only close to the sonic line $k_z = -\omega/c_0$. This is consistent with the fact that the GJW pressure eigenfunctions, predicted for example using a vortex-sheet model [1, 9, 23], have non-negligible amplitudes outside the jet flow only near that line. The levels are, however, not maximum on the line, despite that the normalized magnitude of the pressure eigenfunctions outside the jet tends to one when approaching the limit points of the GJW dispersion curves on the line. Therefore, the amplitudes of the GJW become lower as the GJW are more and more similar to sound waves travelling at the speed of sound.

On the jet axis, in figures 8(a), 9(a) and 10(a), contrary to what is observed at $r = 2r_0$, the levels on the curves are strong everywhere except near the sonic line. This indicates that the amplitude of the GJW inside the jet decreases, as the waves switch from duct-like to free-stream GJW and are less and less confined to the jet flow. This behaviour is in line with the finding of Nogueira et al. [31] that the transmission coefficient of acoustic waves generated in a jet flow to the outside is maximum near the sonic line.

The trends reported above are particularly clear for $M = 0.75$ in figure 8, where the GJW all have a negative group velocity and propagate in the upstream direction. In that case, GJW of modes $n_r = 1$, 2 and 3 appear and can coexist. For $M = 0.95$ and 1.10, in figures 9 and 10, the picture is more complex since the GJW can have negative or positive group velocities and propagate in the upstream or downstream directions. Stationary points, referred to as S_{min} and S_{max} points when they are associated with a local minimum or maximum as illustrated previously in figures 2(b,c), are also found in the dispersion curves. They are at Strouhal numbers $St_D^{Smin,n_r=1} = 0.3495$, $St_D^{Smax,n_r=1} = 0.404$, $St_D^{Smin,n_r=1} = 0.9035$ and $St_D^{Smax,n_r=2} = 0.9715$ for $M = 0.95$, and $St_D^{Smax,n_r=1} = 0.305$ and $St_D^{Smax,n_r=2} = 0.715$ for $M = 1.10$ These points define specific frequency ranges for the GJW of different kinds, delimited by cut-off and/or cut-on frequencies [2, 23]. More surprisingly, the levels around the stationary points seem particularly strong, see for instance in figure 10(b) for the second radial mode.

C. Acoustic levels at $r = 0$ and $r = 2r_0$ upstream and downstream of the source

To quantify the intensities of the GJW, the sound pressure levels (SPL) calculated at $r = 0$ and $r = 2r_0$ at $z = \pm 10r_0$ are plotted as a function of the source Strouhal number in figures 11(a,b) for $M = 0.75$, figures 12(a,b) for $M = 0.95$ and figures 13(a,b) for $M = 1.10$. The SPL at $z = -10r_0$ and $z = 10r_0$ are given in the left and right figures, respectively. They are compared with the SPL obtained without flow at $10r_0$ from the source, SPL_{noflow}, approximately equal to 39 dB. Except in the downstream spectra at low Strouhal numbers where a bump can be attributed to KH instability waves, levels higher than SPL_{noflow} in the simulations reveal the presence of GJW. In contrast, lower levels suggest that the acoustic waves radiated by the source do not generate GJW, but are diverted away from the jet axis by refraction effects. This is notably the case in the upstream spectra at very low Strouhal numbers. Finally, it can be noted that the Strouhal numbers of the points S_{min} and S_{max} specified above are indicated in the figures, when appropriate.

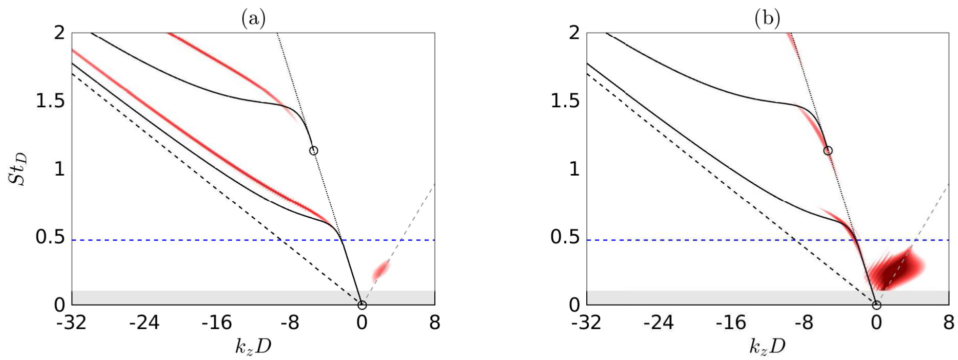

Fig. 8 Representation in the wavenumber-frequency space of the acoustic levels obtained at (a) $r = 0$ and (b) $r = 2r_0$ for $M = 0.75$; ——— GJW dispersion curves for $n_\theta = 0$ at M = 0.75 and ∘ their points L for a vortex sheet; − − − $k_z = \omega/(u_j - c_0)$, ····· $k_z = -\omega/c_0$, − − − $k_z = \omega/(0.7u_j)$; − − − neutral frequency of KH instability waves for $n_\theta = 0$ according to LSA. The levels of the white-to-red color scales spread over 12 dB. There are no simulations in the grey zone.

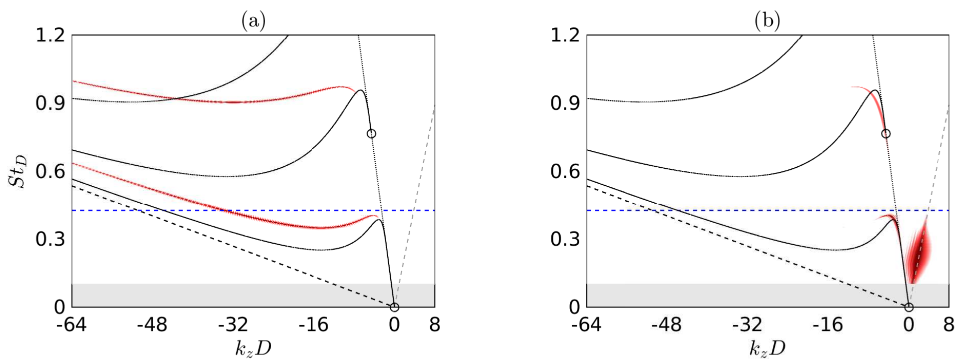

Fig. 9 Representation in the wavenumber-frequency space of the acoustic levels obtained at (a) $r = 0$ and (b) $r = 2r_0$ for $M = 0.95$; ——— GJW dispersion curves for $n_\theta = 0$ at M = 0.95 and ∘ their points L for a vortex sheet; − − − $k_z = \omega/(u_j - c_0)$, ····· $k_z = -\omega/c_0$, − − − $k_z = \omega/(0.7u_j)$; − − − neutral frequency of KH instability waves for $n_\theta = 0$ according to LSA. The levels of the white-to-red color scales spread over 12 dB. There are no simulations in the grey zone.

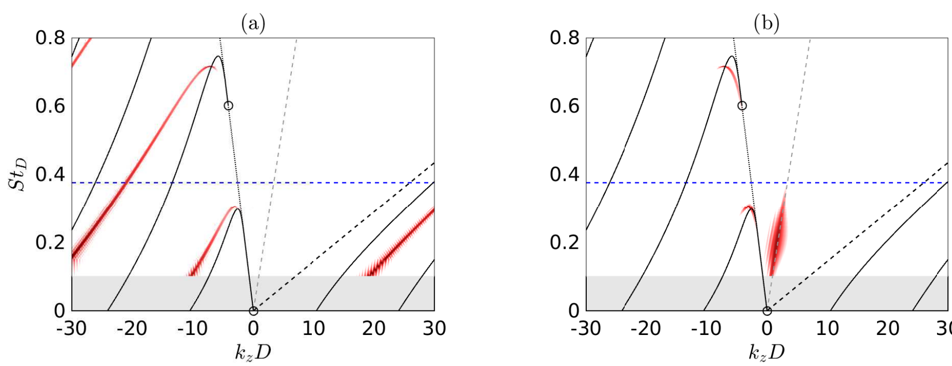

Fig. 10 Representation in the wavenumber-frequency space of the acoustic levels obtained at (a) $r = 0$ and (b) $r = 2r_0$ for $M = 1.10$; ——— GJW dispersion curves for $n_\theta = 0$ at M = 1.10 and ∘ their points L for a vortex sheet; − − − $k_z = \omega/(u_j - c_0)$, ····· $k_z = -\omega/c_0$, − − − $k_z = \omega/(0.7u_j)$; − − − neutral frequency of KH instability waves for $n_\theta = 0$ according to LSA. The levels of the white-to-red color scales spread over 12 dB. There are no simulations in the grey zone.

For $M = 0.75$, at $z = 10r_0$ in figure 11(b), the levels obtained at $r = 0$ and $r = 2r_0$ outside the bump associated with KH instability waves are lower than SPL_{noflow}, as expected given the absence of downstream-propagating GJW. At $z = -10r_0$ in figure 11(a), the levels at $r = 0$ are stronger than SPL_{noflow} for $St_D \geq 0.32$, with a gain greater than 30 dB for $St_D \geq 0.55$, due to the presence of upstream-propagating GJW. The levels at $r = 2r_0$ outside the jet are weaker and, interestingly, oscillate around SPL_{noflow}, showing two humps peaking 12 and 6 dB above SPL_{noflow} at $St_D = 0.57$ and 1.25. These humps result from free-stream GJW belonging to the radial modes $n_r = 1$ and 2. Conversely, when $SPL < SPL_{noflow}$, the GJW are all confined to the flow.

For $M = 0.95$, the levels at $r = 0$ are between 40 and 90 dB stronger than SPL_{noflow} above $St_D^{Smin,n_r=1}$ at $z = -10r_0$ in figure 12(a) and over $St_D^{Smin,n_r=1} \leq St_D \leq St_D^{Smax,n_r=1}$ and $St_D^{Smin,n_r=2} \leq St_D \leq St_D^{Smax,n_r=2}$ at $z = 10r_0$ in figure 12(b). In the first case, the levels vary in a reverse sawtooth manner with sharp rises of 40-50 dB at $St_D^{Smin,n_r=1}$ and $St_D^{Smin,n_r=2}$ followed by gradual decreases. They can be attributed to upstream-propagating duct-like GJW, which are only allowed above the frequencies of the points S_{min} in the GJW dispersion curves. In the second case, the levels in the narrow Strouhal number ranges can be related to downstream-propagating GJW, which can only exist between the frequencies of the stationary points S_{min} and S_{max}. The peak values emerge, nearly as tones, at the Strouhal numbers of these points, suggesting that the GJW with a group velocity close to zero are especially intense.

At $r = 2r_0$, outside the jet, the levels at $z = 10r_0$ are weaker than SPL_{noflow} except in the bump of the KH instability waves, and at $St_D^{Smax,n_r=1}$ and $St_D^{Smax,n_r=2}$. At $z = -10r_0$, they fluctuate in a sawtooth manner with progressive increases followed by sharp falls of 53 dB at $St_D^{Smax,n_r=1}$ and 32 dB at $St_D^{Smax,n_r=2}$, after which the levels are 15-20 dB lower than SPL_{noflow}. In that case, the levels greater than SPL_{noflow} are due to upstream-propagating free-stream GJW, which are cut-off at the frequencies of the points S_{max} in the GJW dispersion curves. Again, tonal peaks are observed at the Strouhal numbers of these points, 34 and 18 dB above SPL_{noflow}.

Finally, for $M = 1.10$, in figure 13(b), the levels at $z = 10r_0$ are all stronger than SPL_{noflow} at $r = 0$, and weaker than SPL_{noflow} at $r = 2r_0$ except in the bump of the KH instability waves and at $St_D^{Smax,n_r=1}$ and $St_D^{Smax,n_r=2}$. This is because duct-like GJW travel in the downstream direction for all frequencies. At $z = -10r_0$, in figure 13(a), the levels at $r = 0$ and $r = 2r_0$ both vary in a sawtooth manner, similarly to the levels at $r = 2r_0$ in figure 12(a), with tonal peaks at $St_D^{Smax,n_r=1}$ and $St_D^{Smax,n_r=2}$, 33 and 29 dB above SPL_{noflow} for $r = 2r_0$. The levels greater than SPL_{noflow} arise from the presence of upstream-propagating GJW, which all have a free-stream nature and are cut-off at the frequencies of the points S_{max} at $M = 1.10$.

In summary, the amplitudes of the GJW inside and outside the jet vary smoothly with the frequency for $M = 0.75$, but in a sharp manner for $M = 0.95$ and 1.10 with tonal-like peaks at the frequencies of the stationary points in the GJW dispersion curves. These trends are consistent with those observed in the near-nozzle spectra of jets at comparable Mach numbers, illustrated in figures 1(a-c) for M = 0.60, 0.90 and 1.10 for instance.

IV. Conclusion

In this paper, the GJW that may exist in jet flow are investigated by solving a problem of acoustic propagation, consisting of a source on the axis of a cylindrical shear layer radiating waves of low amplitude. Three Mach numbers M = 0.75, 0.95 and 1.10, a shear-layer thickness sufficiently large to avoid the development of strong KH instability waves and a wide range of source Strouhal numbers are considered.

In some cases, GJW appear in the jet flow, while in other cases they do not. When they appear, their radial supports and their directions of propagation vary according to the jet Mach number and the source Strouhal number. The variations are explained by representing the levels of the pressure fluctuations inside and outside the jet in the wavenumber-frequency space, thus revealing the dispersion curves of the GJW. The amplitudes of the GJW are then quantified upstream and downstream of the source. As the frequency increases, they fluctuate in a continuous manner for $M = 0.75$ but in a sharp manner with discontinuities and the emergence of tonal-like peaks at the frequencies of the stationary points in the GJW dispersion curves for $M = 0.95$ and 1.10. Outside the jet, in particular, compared with the levels obtained for sound waves propagating in a medium at rest, the peak levels at only 10 jet radii from the source are typically 10 dB higher in the first case but up to 30 dB higher in the second.

The present results provide additional evidence that GJW simply result from the reflection and transmission of acoustic waves generated in a jet [31]. Their very high amplitudes at specific frequencies also further explain why the feedback loops in resonant jets are most often closed by GJW and not by sound waves propagating out of the flow. Finally, the tonal peaks at the frequencies of the stationary points in the GJW dispersion curves for $M = 0.95$ and 1.10 suggest that such peaks can be obtained without the establishment of a resonance phenomenon.

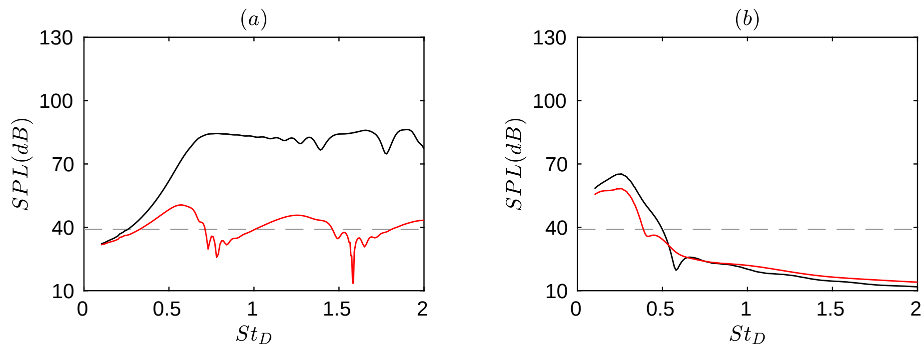

Fig. 11 Variations with the source Strouhal number of the acoustic levels (a) at $z = -10r_0$ and (b) $z = 10r_0$ for $M = 0.75$: —— SPL at $r = 0$, —— SPL at $r = 2r_0$; – – – $SPL_{no\,flow}$.

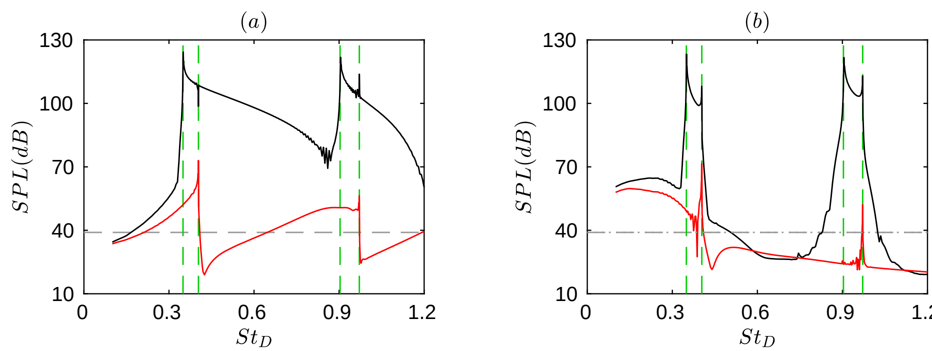

Fig. 12 Variations with the source Strouhal number of the acoustic levels at (a) $z = -10r_0$ and (b) $z = 10r_0$ for $M = 0.95$: —— SPL at $r = 0$, —— SPL at $r = 2r_0$; – – – $SPL_{no\,flow}$; – – – $St_D^{Smin,n_r=1}$, $St_D^{Smax,n_r=1}$, $St_D^{Smin,n_r=2}$ and $St_D^{Smax,n_r=2}$, from left to right.

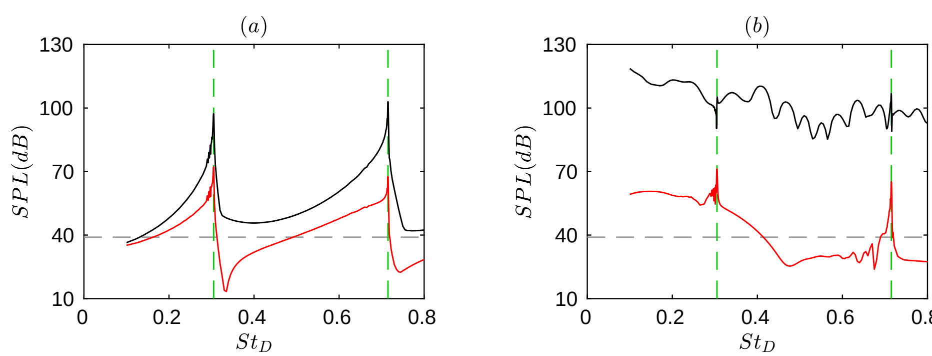

Fig. 13 Variations with the source Strouhal number of the acoustic levels (a) at $z = -10r_0$ and (b) $z = 10r_0$ for $M = 1.10$: —— SPL at $r = 0$, —— SPL at $r = 2r_0$; – – – $SPL_{no\,flow}$; – – – $St_D^{Smax,n_r=1}$ and $St_D^{Smax,n_r=2}$, from left to right.

Acknowledgments

This work was granted access to the HPC resources of PMCS2I (Pôle de Modélisation et de Calcul en Sciences de l'Ingénieur et de l'Information) of Ecole Centrale de Lyon and to the resources of CINES (Centre Informatique National de l'Enseignement Supérieur) and IDRIS (Institut du Développement et des Ressources en Informatique Scientifique) under the allocation 2024-2a0204 made by GENCI (Grand Equipement National de Calcul Intensif). It was performed within the framework of the LABEX CeLyA (ANR-10-LABX-0060) of Université de Lyon, within the program *Investissements d'Avenir* (ANR-16-IDEX-0005) operated by the French National Research Agency (ANR).

References

[1] Tam, C. K. W., and Hu, F. Q., "On the three families of instability waves of high-speed jets," *J. Fluid Mech.*, Vol. 201, 1989, pp. 447–483. https://doi.org/10.1017/S002211208900100X.

[2] Tam, C. K. W., and Norum, T. D., "Impingement tones of large aspect ratio supersonic rectangular jets," *AIAA J.*, Vol. 30, No. 2, 1992, pp. 304–311. https://doi.org/10.2514/3.10919.

[3] Tam, C. K. W., and Ahuja, K. K., "Theoretical model of discrete tone generation by impinging jets," *J. Fluid Mech.*, Vol. 214, 1990, pp. 67–87. https://doi.org/10.1017/S0022112090000052.

[4] Edgington-Mitchell, D., "Aeroacoustic resonance and self-excitation in screeching and impinging supersonic jets - A review," *Int. J. Aeroacoust.*, Vol. 18, No. 2-3, 2019, pp. 118–188. https://doi.org/10.1177/1475472X19834521.

[5] Gojon, R., Bogey, C., and Marsden, O., "Investigation of tone generation in ideally expanded supersonic planar impinging jets using large-eddy simulation," *J. Fluid Mech.*, Vol. 808, 2016, pp. 90–115. https://doi.org/10.1017/jfm.2016.628.

[6] Bogey, C., and Gojon, R., "Feedback loop and upwind-propagating waves in ideally-expanded supersonic impinging round jets," *J. Fluid Mech.*, Vol. 823, 2017, pp. 562–591. https://doi.org/10.1017/jfm.2017.334.

[7] Jaunet, V., Mancinelli, M., Jordan, P., Towne, A., Edgington-Mitchell, D. M., Lehnasch, G., and Girard, S., "Dynamics of round jet impingement," Tech. Rep. 2019-2769, AIAA Paper, 2019. https://doi.org/10.2514/6.2019-2769.

[8] Varé, M., and Bogey, C., "Generation of acoustic tones in round jets at a Mach number of 0.9 impinging on a plate with and without a hole," *J. Fluid Mech.*, Vol. 936, 2022, p. A16. https://doi.org/10.1017/jfm.2022.47.

[9] Jordan, P., Jaunet, V., Towne, A., Cavalieri, A. V. G., Colonius, T., Schmidt, O., and Agarwal, A., "Jet–flap interaction tones," *J. Fluid Mech.*, Vol. 853, 2018, pp. 333–358. https://doi.org/10.1017/jfm.2018.566.

[10] Zaman, K. B. M. Q., Fagan, A. F., Bridges, J. E., and Brown, C. A., "An experimental investigation of resonant interaction of a rectangular jet with a flat plate," *J. Fluid Mech.*, Vol. 779, 2015, pp. 751–775. https://doi.org/10.1017/jfm.2015.453.

[11] Tam, C. K. W., and Chandramouli, S., "Jet-plate interaction tones relevant to over-the-wing engine mount concept," *J. Sound Vib.*, Vol. 486, 2020, p. 115378. https://doi.org/10.1016/j.jsv.2020.115378.

[12] Gojon, R., Bogey, C., and Mihaescu, M., "Oscillation modes in screeching jets," *AIAA J.*, Vol. 56, No. 7, 2018, pp. 2918–2924. https://doi.org/10.2514/1.J056936.

[13] Edgington-Mitchell, D., Jaunet, V., Jordan, P., Towne, A., Soria, J., and Honnery, D., "Upstream-travelling acoustic jet modes as a closure mechanism for screech," *J. Fluid Mech.*, Vol. 855, 2018, p. R1. https://doi.org/10.1017/jfm.2018.642.

[14] Mancinelli, M., Jaunet, V., Jordan, P., and Towne, A., "Screech-tone prediction using upstream-travelling jet modes," *Exp Fluids*, Vol. 60, No. 1, 2019, p. 22. https://doi.org/10.1007/s00348-018-2673-2.

[15] Nogueira, P., and Edgington-Mitchell, D., "Investigation of supersonic twin-jet coupling using spatial linear stability analysis," *J. Fluid Mech.*, Vol. 918, 2021, p. A38. https://doi.org/10.1017/jfm.2021.366.

[16] Suzuki, T., and Colonius, T., "Instability waves in a subsonic round jet detected using a near-field phased microphone array," *J. Fluid Mech.*, Vol. 565, 2006, pp. 197–226. https://doi.org/10.1017/S0022112006001613.

[17] Brès, G. A., Jordan, P., Jaunet, V., Le Rallic, M., Cavalieri, A. V. G., Towne, A., Lele, S. K., Colonius, T., and Schmidt, O. T., "Importance of the nozzle-exit boundary-layer state in subsonic turbulent jets," *J. Fluid Mech.*, Vol. 851, 2018, pp. 83–124. https://doi.org/10.1017/jfm.2018.476.

[18] Bogey, C., “Acoustic tones in the near-nozzle region of jets: characteristics and variations between Mach numbers 0.5 and 2,” *J. Fluid Mech.*, Vol. 921, 2021, p. A3. https://doi.org/10.1017/jfm.2021.426.

[19] Zaman, K. B. M. Q., Fagan, A. F., and Upadhyay, P., “Pressure fluctuations due to ‘trapped waves’ in the initial region of compressible jets,” *J. Fluid Mech.*, Vol. 931, 2022, p. A30. https://doi.org/10.1017/jfm.2021.954.

[20] Bogey, C., “Tones in the acoustic far field of jets in the upstream direction,” *AIAA J.*, Vol. 60, No. 4, 2022, pp. 2397–2406. https://doi.org/10.2514/1.J061013.

[21] Zaman, K. B. M. Q., Fagan, A. F., and Upadhyay, P., “Pressure fluctuation spectral peaks due to ’guided waves’ in regions upstream of the jet exit,” Tech. Rep. 2023-3649, AIAA Paper, 2023. https://doi.org/10.2514/6.2023-3649.

[22] Zaman, K., Bridges, J., Upadhyay, P., and Brown, C., “’Trapped wave’ resonance tones radiated in the forward arc of high-speed jets,” Tech. Rep. 20240009873, NASA TM, 2004.

[23] Towne, A., Cavalieri, A. V. G., Jordan, P., Colonius, T., Schmidt, O., Jaunet, V., and Brès, G. A., “Acoustic resonance in the potential core of subsonic jets,” *J. Fluid Mech.*, Vol. 825, 2017, pp. 1113–1152. https://doi.org/10.1017/jfm.2017.346.

[24] Schmidt, O., Towne, A., Colonius, T., Cavalieri, A. V. G., Jordan, P., and Brès, G. A., “Wavepackets and trapped acoustic modes in a turbulent jet: Coherent structure eduction and global stability,” *J. Fluid Mech.*, Vol. 825, 2017, pp. 1153–1181. https://doi.org/10.1017/jfm.2017.407.

[25] Prinja, R., Martini, E., Jordan, P., Towne, A., and Cavalieri, A. V. G., “Wave reflections and resonance in a Mach 0.9 turbulent jet,” *Theor. Comput. Fluid Dyn.*, Vol. 39, 2025, p. 2. https://doi.org/10.1007/s00162-024-00722-0.

[26] Bogey, C., “Interactions between upstream-propagating guided jet waves and shear-layer instability waves near the nozzle of subsonic and nearly ideally expanded supersonic free jets with laminar boundary layers,” *J. Fluid Mech.*, Vol. 949, 2022, p. A41. https://doi.org/10.1017/jfm.2022.776.

[27] Edgington-Mitchell, D., and Nogueira, P. A. S., “The guided-jet mode in compressible jets,” Tech. Rep. 2023-3647, AIAA Paper, 2023. https://doi.org/10.2514/6.2023-3647.

[28] Maia, I. A., Fiore, M., and Gojon, R., “Tones and upstream-traveling waves in ideally expanded round impinging jets,” *Phys. Rev. Fluids*, Vol. 9, No. 8, 2024, p. 083904. https://doi.org/10.1103/PhysRevFluids.9.083904.

[29] Bogey, C., “Gain in efficiency of jet receptivity to acoustic disturbances with increasing nozzle-lip thickness,” *J. Fluid Mech.*, Vol. 997, 2024, p. A71. https://doi.org/10.1017/jfm.2024.849.

[30] Martini, E., Cavalieri, A. V. G., and Jordan, P., “Acoustic modes in jet and wake stability,” *J. Fluid Mech.*, Vol. 867, 2019, pp. 804–834. https://doi.org/10.1017/jfm.2019.148.

[31] Nogueira, P. A. S., Cavalieri, A. V. G., Martini, E., Towne, A., Jordan, P., and Edgington-Mitchell, D., “Guided-jet waves,” *J. Fluid Mech.*, Vol. 999, 2024, p. A47. https://doi.org/10.1017/jfm.2024.797.

[32] Michalke, A., “Survey on jet instability theory,” *Prog. Aerosp. Sci.*, Vol. 21, 1984, pp. 159–199. https://doi.org/10.1016/0376-0421(84)90005-8.

[33] Bogey, C., “On noise generation in low Reynolds number temporal round jets at a Mach number of 0.9,” *J. Fluid Mech.*, Vol. 859, 2019, pp. 1022–1056. https://doi.org/10.1017/jfm.2018.864.

[34] Bogey, C., and Pineau, P., “Potential-core closing of temporally developing jets at Mach numbers between 0.3 and 2: Scaling and conditional averaging of flow and sound fields,” *Phys. Rev. Fluids*, Vol. 4, No. 12, 2019, p. 124601. https://doi.org/10.1103/PhysRevFluids.4.124601.

[35] Mohseni, K., and Colonius, T., “Numerical treatment of polar coordinate singularities,” *J. Comput. Phys.*, Vol. 157, No. 2, 2000, pp. 787–795. https://doi.org/10.1006/jcph.1999.6382.

[36] Bogey, C., and Bailly, C., “A family of low dispersive and low dissipative explicit schemes for flow and noise computations,” *J. Comput. Phys.*, Vol. 194, No. 1, 2004, pp. 194–214. https://doi.org/10.1016/j.jcp.2003.09.003.

[37] Berland, J., Bogey, C., Marsden, O., and Bailly, C., “High-order, low dispersive and low dissipative explicit schemes for multiple-scale and boundary problems,” *J. Comput. Phys.*, Vol. 224, No. 2, 2007, pp. 637–662. https://doi.org/10.1016/j.jcp.2006.10.017.

[38] Tam, C. K. W., and Dong, Z., “Radiation and outflow boundary conditions for direct computation of acoustic and flow disturbances in a nonuniform mean flow,” *J. Comput. Acous.*, Vol. 4, No. 2, 1996, pp. 175–201. https://doi.org/10.1142/S0218396X96000040.